Tellus (1993), *45A*, 44–53

Dynamics of a two-dimensional ribbon of shallow water on an f-plane

By CHRISTOPH FREI, *Atmospheric Physics, ETH, Hönggerberg, CH-8093 Zürich, Switzerland*

(Manuscript received 27 January 1992; in final form 4 May 1992)

ABSTRACT

An analytical solution is derived for the motion of an infinitely long fluid ribbon of shallow water, with parabolic depth and linear velocity distribution. The solution is of intrinsic dynamical interest and also offers a "bench-mark" for testing numerical methods which handle the intersection of a free surface with a horizontal boundary. The development is expressed in terms of the translation and deformation of the hump. The former component is determined uniquely by the initial velocity at the symmetry axis and the externally imposed uniform pressure gradient. On the other hand, the deformation component depends on the initial shear and divergence, but is unaffected by a uniform external pressure force. Relative to its axis, the fluid ribbon alternately expands and contracts, with a pulsation frequency ($\geqslant$ the inertial frequency f) that is a function of a Rossby, and a rotational Froude number, defined in terms of the initial velocity, and height field.

1. Introduction

The shallow water system of equations offers an amenable and fertile paradigm for many geophysical flow systems ranging from global-tidal theory (Laplace, 1799, 1825), barotropic large scale motion of the atmosphere (Phillips, 1954), frontal instability and movement (e.g., Orlanski, 1968; Davies, 1984), hydraulic flow over terrain (Houghton and Kasahara, 1968), to breaking waves on a beach. In these applications, the shallow water system captures the dynamical essence of some particular phenomenon, renders tractable the mathematics of the problem and hence has promoted our understanding of the often physically complex system. If an analytical solution is obtained for the particular problem in question, then that solution can form an appropriate bench-mark to test numerical models designed to examine much more generalized aspects of the particular phenomenon. This strategy of using the shallow water system as a paradigm is followed here. Bounded masses of heavy (light) fluid at the base (top) of a fluid domain are a common occurrence in geophysical fluids. Our interest here is in fluid segments that are large enough for the influence of the earth's rotation to be significant, e.g., sub-synoptic and meso-α scale bands of cold air linked to fronts, to orographic trapping or to squall line generated downdroughts.

Several investigations of bounded shallow water segments have been undertaken in the past. Ball (1963) derived and documented some general properties for the evolution of arbitrary shaped shallow water layers of limited horizontal extent. He showed that the motion of such a fluid segment, released on a rotating paraboloid, is a superposition of three modes: the displacement of the centre of gravity (which is a linear problem, independent of the deforming motions within the fluid), the distension (characterized by a velocity field with time-dependent but homogeneous divergence and vorticity), and the "additional" deformations, which are governed by shallow water equations with transformed space and time coordinates. Also he noted that the temporal evolution of the distension component is governed by a simple harmonic oscillation of the total moment of inertia. In the case of a flat base, this mode represents an alternating expansion and contraction of the layer, with the inertial frequency f of the background rotation.

Again in the context of oceanic warm-core rings, Cushman-Roisin (1987) derived a particular class of analytical solutions for a shallow water lens. When the depth profile of the elliptic shaped lens is assumed parabolic and the velocity distribution is linear, the evolution is described by a translation, an inertial pulsation and a rotation of the whole vortex. These three components can be identified with the three modes in Ball's general theory.

In this study, to investigate the two-dimensional analogue of the foregoing problem, we adopt a similar spatial structure for the layer depth and velocity to that of the former study, and seek to derive an analogous analytical solution for the evolution of an infinitely long fluid ribbon. This particular flow configuration violates the condition of boundedness, and thus the previous general three-dimensional theory is inapplicable. In particular the distension mode must take a different form, since a moment of inertia cannot be defined for an infinitely elongated strip.

In Section 2, we outline the solution procedure and separate the translation and deformation components of the ridge. Thereafter the temporal change of the layer is discussed in qualitative terms and solved explicitly in Section 3. In view of the foregoing, it is of particular interest to discuss the period of the pulsation mode, analyzed in the fourth section.

2. Separation of displacement and deformation

The flow configuration under study is outlined in Fig. 1. A two-dimensional ribbon of incompressible "shallow water" is located on a flat surface in a rotating coordinate system. The y-axis is aligned parallel to this ridge of fluid and diffusive processes are neglected. Thus the governing equations take the form,

$$\frac{\mathrm{D}u}{\mathrm{D}t} - fv = -g\frac{\partial h}{\partial x} - P_x, \tag{1a}$$

$$\frac{\mathrm{D}v}{\mathrm{D}t} + fu = -P_y, \tag{1b}$$

$$\frac{\mathrm{D}h}{\mathrm{D}t} + h\frac{\partial u}{\partial x} = 0, \tag{1c}$$

where

$$\frac{\mathrm{D}}{\mathrm{D}t} = \frac{\partial}{\partial t} + u\frac{\partial}{\partial x}.$$

and (u, v, h) denote respectively the velocity components and the fluid depth. P_x, P_y signify the acceleration due to a uniform external pressure

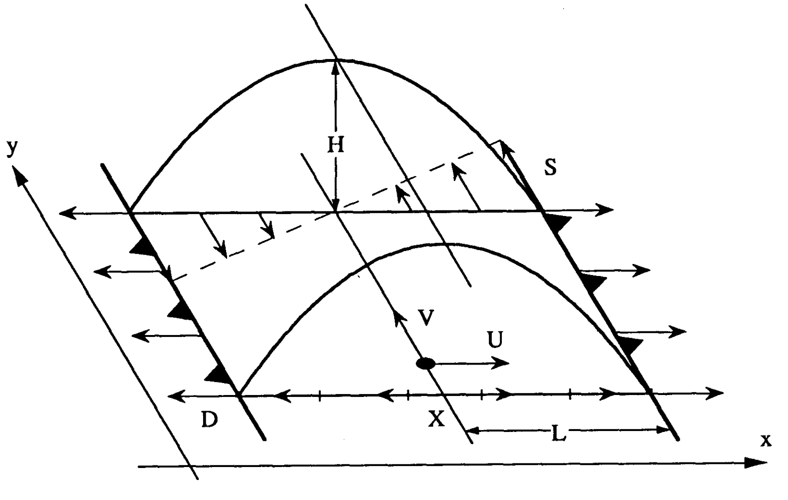

Fig. 1. Profile of the parabolic fluid ridge, with central depth H and the half-width L. Arrows indicate the mean-(U, V) and the relative (D, S) velocity fields.

gradient, or equivalently a uniform terrain slope of the underlying surface.

The fluid layer and flow motion is given a prescribed geometrical shape, i.e., the depth profile is assigned a parabolic shape (c.f. analogous to that of the three dimensional elliptic lens (Cushman-Roisin, 1987)), and the velocity components are assumed to vary linearly across the hump, such that:

$$h(x, t) = H(t)\left(1 - \left(\frac{x - X(t)}{L(t)}\right)^2\right), \tag{2a}$$

$$u(x, t) = U(t) + D(t)\left(\frac{x - X(t)}{L(t)}\right), \tag{2b}$$

$$v(x, t) = V(t) + S(t)\left(\frac{x - X(t)}{L(t)}\right). \tag{2c}$$

The parameters ($X(t)$, $U(t)$, $V(t)$, $H(t)$, $L(t)$, $D(t)$, $S(t)$) are functions of time only, and together they specify the state of the fluid (see Fig. 1): H denotes the central height and L the half-width of the fluid hump. X, U, V are the position and the velocity components of a fluid column on the symmetry axis of the ridge, and the coefficients D, S represent the divergent and shear components in the velocity field. Note that the statements (2) imply homogeneous divergence of value (D/L) and vorticity of value (S/L) across the fluid. If there exist time dependent functions for these parameters to solve the shallow water equations (1), then these functions determine the evolution of a fluid ridge, initially released with parabolic shape and linear velocity field.

On introducing the flow specification (2) into the governing equations (1) and equaling the coefficients for equal powers of the spatial coordinate x, yields the following set of ordinary differential equations:

$$X_t = U, \tag{3.1a}$$

$$U_t - fV = -P_x, \tag{3.1b}$$

$$V_t + fU = -P_y, \tag{3.1c}$$

$$L_t = D, \tag{3.2a}$$

$$\frac{H_t}{H} = -\frac{D}{L}, \tag{3.2b}$$

$$S_t + fD = 0, \tag{3.2c}$$

$$D_t - fS = 2g\frac{H}{L}. \tag{3.2d}$$

Here the subscript $_t$ denotes the temporal derivative. We obtain 7 equations for the 7 dependent functions (X, U, V, L, H, S and D). This well-posed problem confirms the consistency of the prescriptions (2) for the shallow water system.

The set of differential equations (3) can be split in two decoupled parts. First eqs. (3.1a–c) involve only parameters determining the motion of the symmetry axis and describe the response of the entire hump to the external pressure gradient. On the other hand the nonlinear set (3.2) describes the deformation of the fluid and the changes in divergence and vorticity, that accompany the release of potential energy during the collapse of the hump. It follows that changes in the shape do not influence the movement of the symmetry axis, and that the external pressure gradient does not affect the internal deformation.

The linear displacement problem (3.1) can be readily solved, if the pressure force (P_x, P_y) is time-independent:

$$U(t) + \frac{P_y}{f} = A\sin(f(t+T)),$$

$$V(t) - \frac{P_x}{f} = A\cos(f(t+T)),$$

i.e., the velocity components at the symmetry axis oscillate about a geostrophic equilibrium state (i.e., $U = -P_y/f$, $V = P_x/f$), with an amplitude A and a phase T determined by the initial conditions. The motion of a fluid column on the symmetry axis is given by the superposition of an oscillation and a uniform translation perpendicular to the external pressure gradient.

3. Deformation under gravity and rotation

For a coordinate system advecting with the fluid parcels located on the symmetry axis of the ridge, the flow evolution is determined by the nonlinear initial value problem posed by eqs. (3.2). To examine this deformation component of the dynamics, we adopt the following scaled parameters,

$$\lambda = \frac{L(t)}{L_0}, \qquad \eta = \frac{H(t)}{H_0}, \qquad \sigma = \frac{S(t)}{fL_0},$$

$$\delta = \frac{D(t)}{fL_0}, \qquad \tau = ft.$$

Here the zero subscript refers to the initial configuration, λ and η denote respectively the fluid extension and the central depth, and σ, δ represent the fluid velocity components at the front-ground intersection. Note also that the time has been non-dimensionalized in terms of the inertial period.

With the use of the non-dimensional variables the differential eqs. (3.2) take the form:

$$\lambda_\tau = \delta, \tag{4a}$$

$$\frac{\eta_\tau}{\eta} = -\frac{\delta}{\lambda}, \tag{4b}$$

$$\sigma_\tau + \delta = 0, \tag{4c}$$

$$\delta_\tau - \sigma = \mathscr{F}^2 \frac{\eta}{\lambda}, \tag{4d}$$

and the initial values and parameters are defined by:

$$\lambda_0 = 1, \qquad \eta_0 = 1, \qquad \sigma_0 = \mathscr{R}_y = \frac{S_0}{fL_0},$$

$$\delta_0 = \mathscr{R}_x = \frac{D_0}{fL_0}, \qquad \mathscr{F} = \frac{\sqrt{2gH_0}}{fL_0}.$$

Here the external parameters are given by $\mathscr{R}_x$ and $\mathscr{R}_y$ the Rossby-numbers and $\mathscr{F}$ is the inverse of a rotational Froude-number or a nondimensional Rossby radius of deformation.

Eq. (4a) insures, that at the layer intersections with the rigid surface the fluid movement is consistent with that of the adjacent fluid, a necessary requirement in shallow water dynamics. Using (4a) to substitute δ, each of the remaining equations can be integrated separately to yield the three conservation laws for the liquid volume, the potential vorticity and the energy:

$$\lambda \cdot \eta \equiv 1, \qquad \text{(liquid volume)}, \tag{5a}$$

$$\frac{1 + \sigma/\lambda}{\eta} \equiv 1 + \mathscr{R}_y, \qquad \text{(potential vorticity)}, \tag{5b}$$

$$\frac{\delta^2 + \sigma^2}{2} + \eta \cdot \mathscr{F}^2 \equiv \frac{\mathscr{R}_x^2 + \mathscr{R}_y^2}{2} + \mathscr{F}^2 \qquad \text{(energy)}, \tag{5c}$$

On the right-hand side the conserved quantities are expressed by means of the parameters for the initial conditions $\mathscr{R}_x$, $\mathscr{R}_y$ and $\mathscr{F}$.

Using eqs. (5a, b) to substitute the dimensionless height η and shear velocity σ, the energy conservation (5c) can be expressed in terms of one single dependent variable (i.e., the ridge expansion λ):

$$\lambda \cdot \lambda_\tau^2 = (\lambda - 1) \cdot (\lambda_+ - \lambda) \cdot (\lambda - \lambda_-) + \lambda \cdot \mathscr{R}_x^2, \tag{6}$$

where λ_+ and λ_- are real quantities:

$$\begin{aligned} \lambda_+ &= (\tfrac{1}{2} + \mathscr{R}_y) + \sqrt{(\tfrac{1}{2} + \mathscr{R}_y)^2 + 2\mathscr{F}^2} > 0, \\ \lambda_- &= (\tfrac{1}{2} + \mathscr{R}_y) - \sqrt{(\tfrac{1}{2} + \mathscr{R}_y)^2 + 2\mathscr{F}^2} < 0. \end{aligned} \tag{7}$$

The right-hand side of this ordinary differential equation is a polynomial of third order and (6) can be written in the form:

$$\lambda \cdot \lambda_\tau^2 = (\lambda - \lambda_1) \cdot (\lambda_2 - \lambda) \cdot (\lambda - \lambda_3) \tag{6'}$$

if we define λ_1, λ_2, and λ_3 as the roots of the referred polynomial.

The representations (6) and (6′) for the product $\lambda \cdot \lambda_\tau^2$ offer the possibility of tracing the evolution of the fluid ridge in a qualitative manner:

First note, that whatever the physical configuration of the hump, the term $\lambda \cdot \lambda_\tau^2$ is always positive or zero. The physical state of the ridge during its evolution is thus restricted to a range of expansions λ, corresponding to the cubic polynomial on the right-hand side of (6′) being positive or zero. This range can be identified and hence it determines basic properties of the polynomial roots λ_1, λ_2, and λ_3:

From (6), it is seen that in the special case of a divergence free initial state (i.e., $\mathscr{R}_x = 0$), all three roots are real. Two are positive (i.e., 1, λ_+) and one is negative (i.e., λ_-). Furthermore for ridge expansions between the positive roots ($1 < \lambda < \lambda_+$) the polynomial takes positive values. Analogous properties can be derived when initial divergence is present: The inclusion of the linear term $\lambda \cdot \mathscr{R}_x^2$ in eq. (6) does not alter the sign of the polynomial roots and therefore all three roots λ_1, λ_2, and λ_3 are real and satisfy the relationships $\lambda_3 < 0 < \lambda_1 \leqslant 1 \leqslant \lambda_2$. Thus the right-hand side of eq. (6), and equivalently eq. (6′), is positive for ridge expansions between the positive roots: $\lambda_1 \leqslant \lambda \leqslant \lambda_2$.

These deduced properties of the polynomial in eq. (6) serve to aid the visualization of the flow succession in the phase space, i.e., the diagram where the front velocity is plotted against the actual ridge width. Such a sample trajectory $\lambda_\tau(\lambda)$ is shown in Fig. 2. Following the above discussion, the trace is restricted to widths between the

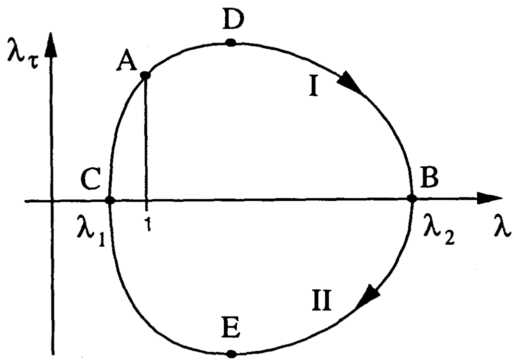

Fig. 2. Schematic trajectory in the phase space of the expansion (I) and contraction (II) of the fluid ridge on a rotating plane.

extreme values λ_1 and λ_2, but in this range it consists of two symmetric branches, joining one another at λ_1 and λ_2 on the λ-axis. During the deformation, the state of the ridge follows the resulting curve clockwise: For instance starting with a state of positive initial divergence at A (Fig. 2), the phase space state of the ridge follows the upper branch until maximal expansion is reached at B. Because the trajectory approaches the λ-axis at a right angle, a state of stagnation will be achieved within a finite time interval. Thereafter the expansion is reversed to a contraction, and the fluid state traces back along the bottom branch. After a while the inner turning point C with the minimal width λ_1 will be reached, and from there the system is proceeding to the upper branch again. Consequently the hump deforms itself periodically, expanding and contracting between the extreme widths λ_1 and λ_2. The balance states D and E, where gravitational expansion and restoring Coriolis force cancel each other, are never achieved as equilibrium configurations, because divergence and convergence increase to these points and therefore the divergent flow components attain the maximum values at D and E. There is one special case however when $\lambda_1 = \lambda_2 = 1$; i.e., when the fluid got released in geostrophic balance: $\mathscr{R}_y = -\mathscr{F}^2$, $\mathscr{R}_x = 0$. The phase space trajectory degenerates to a point for this singular setting.

We can conclude, that for any initial configuration, specified by the three parameters $\mathscr{R}_x$, $\mathscr{R}_y$, and $\mathscr{F}$, there exist two extreme widths of the ridge, where the deformation momentarily stagnates. Hence every dynamical evolution of the hump can be achieved, releasing the hump from a divergence free initial state (i.e., $\mathscr{R}_x = 0$). In the on-going discussion we will concentrate ourselves to this special subclass of initial configurations. This does not restrict the variety of flow successions, but it simplifies the analysis, since the extreme widths $\lambda = 1$, $\lambda = \lambda_+$ can be expressed analytically (see eq. 7). Furthermore the full diversity of solutions is then confined to a two-dimensional parameter half-plane spanned by ($\mathscr{R}_y$, $\mathscr{F} > 0$).

On the basis of function $\lambda_\tau(\lambda)$ in (6), the final integration step can be performed and will determine the quantitative evolution of the width λ after the ridge has been released from a divergence free initial state. The formal integration leads to an expression for the dimensionless time τ, that expires until the ridge attains a certain width λ:

$$\tau(\lambda) = \int_1^\lambda \frac{\mathrm{d}\lambda' \sqrt{\lambda'}}{\sqrt{(\lambda' - 1)(\lambda_+ - \lambda')(\lambda' - \lambda_-)}}. \tag{8}$$

Here the right-hand side is recognized as an elliptic integral and by virtue of the substitution

$$\sin \varphi = \sqrt{\frac{\lambda_+ \cdot (\lambda - 1)}{(\lambda_+ - 1) \cdot \lambda}}, \tag{9}$$

it can be transformed to the standard representation for elliptic integrals (Byrd and Friedman, 1954). Then the general analytic solution for the lapse time can be expressed concisely as

$$\tau(\lambda) = \gamma \cdot \Pi(n, \varphi(\lambda), m^2), \tag{10}$$

where

$$\gamma = \frac{2}{\sqrt{\lambda_+(1 - \lambda_-)}}, \tag{11}$$

and Π is the elliptic integral of third kind:

$$\Pi(n, \varphi, m^2) = \int_0^\varphi \frac{\mathrm{d}\varphi'}{(1 - n \sin^2 \varphi') \sqrt{1 - m^2 \sin^2 \varphi'}}, \tag{12}$$

where m and n are respectively the modulus and the parameter of Π, defined by:

$$m^2 = \frac{(\lambda_+ - 1)(-\lambda_-)}{\lambda_+(1 - \lambda_-)}, \qquad n = \frac{\lambda_+ - 1}{\lambda_+}. \tag{13}$$

To determine the evolution for a particular initial state, the starting configuration has to be introduced into λ_+ and λ_- (eq. 7) via the definitions for $\mathscr{R}_y$ and $\mathscr{F}$. Subsequently the integration of (8) or alternatively (10) can be performed numerically. Using the elliptic form (10) has the advantage, that the integrand has no poles in the integration domain, and hence the numerical calculation converges rapidly. There is however the restriction that (10) only applies for motions along the expanding branch (I) of the phase space, but note the symmetry between the contracting and expanding phases.

4. The period of the deformation cycle

It was inferred from the phase space considerations in the previous section that the combined effect of gravity and rotation upon a parabolic shallow water ridge gives rise to a periodic extension and contraction of the ridge. In this section we will interpret the measure of the period associated with this pulsation. Since the period is linked to two characteristic time scales, related to rotation and gravitation, it is instructive to first discuss the deformation of the ridge subject to these two forces in isolation:

As a basis we use the equation of motion (4d) and substitute δ, σ and η from (4a), (5b) and (5a). This yields a second order equation for the half width λ:

$$\lambda_{\tau\tau} = \underbrace{-((\lambda-1)-\mathscr{R}_y)}_{\text{Rot}} + \underbrace{\mathscr{F}^2\frac{1}{\lambda^2}}_{\text{Grav}}, \tag{14}$$

where on the right-hand side the Coriolis and gravitation forcing appear separated as the first and second term respectively. Omitting either of the two and integrating will yield the purely rotational and the purely gravitational deformation of the fluid ridge. The results are as follows:

In the non-rotating limit, the fluid ridge expands continuously and the time scale:

$$t_g = \frac{1}{\sqrt{2}\,\mathscr{F}f} = \frac{L_0}{\sqrt{2gH_0}}$$

appears as a natural time measure for this purely gravitational collapse. After the expiry of many

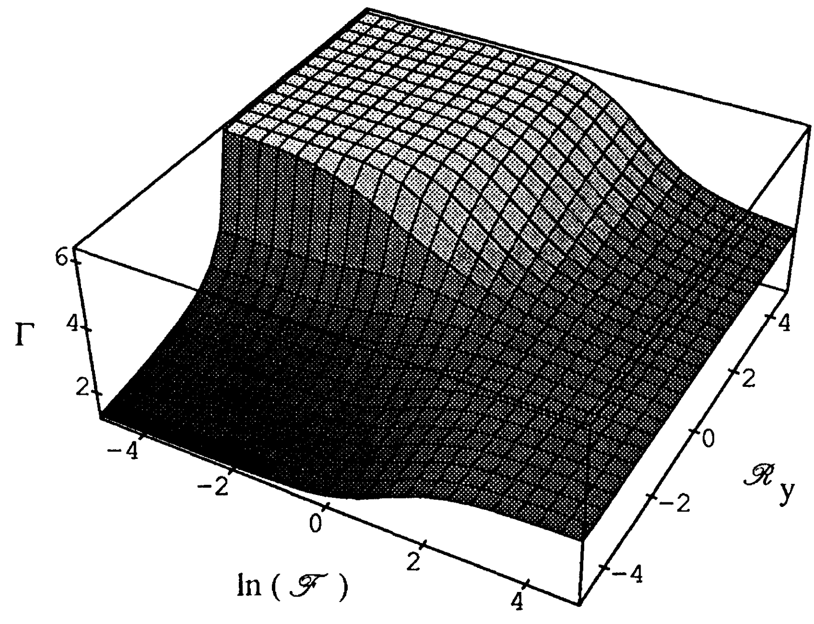

Fig. 3. The non-dimensionalised period Γ of the system's deformation cycle, displayed in the parameter space $\{\ln(\mathscr{F}), \mathscr{R}_y\}$.

gravitational time units ($t \gg t_g$), the spread becomes quasi-stationary, and the front speed approaches the asymptotic velocity:

$$\delta_\infty = \sqrt{2}\,\mathscr{F} \Leftrightarrow D_\infty = 2\sqrt{gH_0}. \tag{15}$$

Considering the Coriolis force in isolation, then the motion of the fluid ridge would be a harmonic oscillation, provided there is a shear component present in the initial flow field (i.e., $\sigma_0 \neq 0$). The frequency of the oscillation is the inertial frequency f and the maximal- and minimal expansions are:

$$\begin{aligned} \lambda_{\max} &= 1 + \mathscr{R}_y + \sqrt{\mathscr{R}_x^2 + \mathscr{R}_y^2} \\ \lambda_{\min} &= 1 + \mathscr{R}_y - \sqrt{\mathscr{R}_x^2 + \mathscr{R}_y^2}. \end{aligned} \tag{16}$$

In the mixed case now, the resulting oscillation is no more harmonic and its frequency depends on the initial conditions. The dimensionless period Γ of the cycle is determined by:

$$\Gamma(\mathscr{R}_y, \mathscr{F}) = 2\gamma \cdot \Pi\left(n, \frac{\pi}{2}, m^2\right). \tag{17}$$

Fig. 3 depicts the period Γ calculated from (17) as a surface in the parameter space of the Rossby number and inverse rotational Froude number ($\mathscr{R}_y$, $\ln(\mathscr{F})$). It is evident that the deformation period has an upper limit at 2π, the dimensionless measure for one period of the background rotation. Thus irrespective of the initial configuration, the pulsation cycle is *faster* than the displacement of the whole ridge. Moreover the step like shape of Γ suggests that the set of solutions to (14) falls into three broad categories, each typified by different characteristic deformation periods:

For positive Rossby numbers and inverse Froude numbers considerably smaller than 1, i.e., the upper left of the parameter plane, the flow response is quasi-inertial. For such configurations Coriolis effects account for the major part of the acceleration, and the gravitational effect remains small throughout (i.e., Rot $\gg$ Grav in (14)). It follows that a quasi-inertial period is realized. The minor impact of the gravitation to the flow evolution is illustrated in Fig. 4a. It shows the typical phase space track (expanding branch) for this parameter domain along with the corresponding result when the gravitational effect is not present (i.e., $\mathscr{F} = 0$).

To interpret flow dynamics associated with large

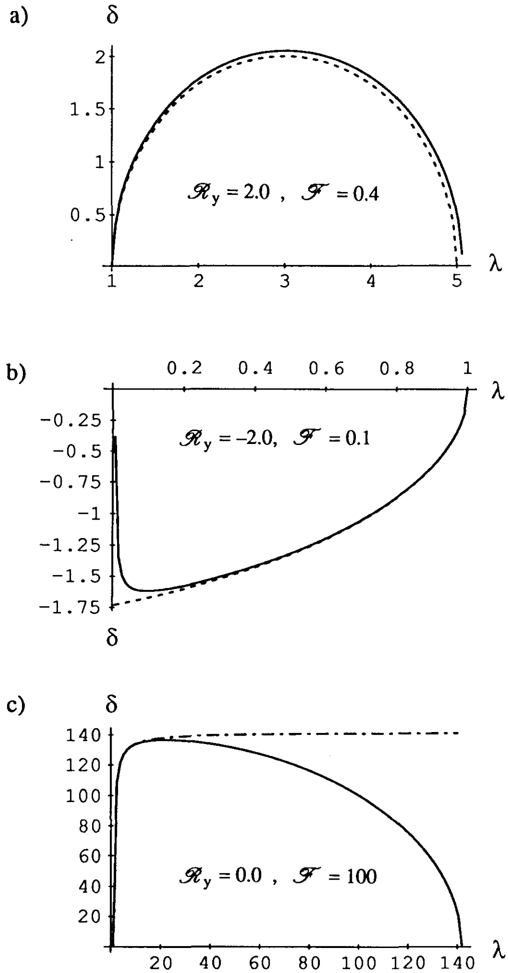

Fig. 4. Sample traces in the phase space (expansion velocity δ against actual width λ) of the deformation of a fluid ridge in a rotating frame; full line, gravitational and rotational effects included; dashed line, only rotational forcing; dash-dotted line, only gravitational forcing. Displayed cases correspond to typical settings for the three regimes of the deformation period: (a) $\mathscr{R}_y = 2.0$, $\mathscr{F} = 0.4$. (b) $\mathscr{R}_y = -2.0$, $\mathscr{F} = 0.1$. (c) $\mathscr{R}_y = 0.0$, $\mathscr{F} = 100$.

negative values of $\mathscr{R}_y$ and small values of $\mathscr{F}$ (i.e., the lower left of the parameter plane in Fig. 3), recall that a pure inertial oscillation is accompanied with the extreme half-widths of 1 and $1 + 2\mathscr{R}_y$ (see eq. (16)). In the absence of potential energy, the Coriolis accelerations would seek to drive the fluid ridge to unphysical negative widths as far as $\mathscr{R}_y < -0.5$. However the gravitational effect, despite the smallness of $\mathscr{F}$, will become significant and then dominate as the ridge tightens. This process is illustrated in Fig. 4b, which shows the trajectories in phase space (contracting branch) for the setting $\mathscr{R}_y = -2.0$, $\mathscr{F} = 0.1$ and the corresponding pure inertial oscillation. Commencing at $\lambda = 1$ the fluid ridge contracts due to the strong negative shear, but as $\lambda \to 0$ the contraction is stopped and finally reversed. In harmony with Fig. 3, the realized deformation periods will be some fraction of the inertial value and this fraction depends upon how much of the inertial oscillation between $\lambda = 1$ and $\lambda = 1 + 2\mathscr{R}_y$ is cut at $\lambda \approx 0$.

The third distinctive dynamical regime is found at large inverse Froude numbers $\mathscr{F} \gg 1$ with $\mathscr{F} \gg \mathscr{R}_y$. An example of a phase space curve for this domain is shown in Fig. 4c, along with the solution for the non-rotating case. It is apparent that initially the expansion is substantially accelerated by the conversion of potential energy. This persists until the front velocity attains the pure gravitational limit δ_∞ (eq. (15)). Thereafter the rate of expansion levels off, but the continuing spread with the rotation induces shear along the ridge. This, in turn, results in a restoring Coriolis effect. At this stage, there is a sharp transition from gravitationally dominated to a rotationally dominated flow, attributable to the different power laws in the rotation and gravitation term of eq. (14). This transition can be viewed as the initiation of an inertial oscillation with the initial condition $\delta_\tau = 0$. From now on the ridge expands and recontracts according to the rotationally dominated flow regime, until after approximately half an inertial period, the reverse transition occurs on the contracting branch of the phase space track. However since the gravitational time scale t_g is small compared to f^{-1} in this regime, the forementioned half inertial cycle constitutes the main contribution to the pulsation period. It follows that for this part of the parameter space the Γ surface in Fig. 3 levels off at a value of π.

Fig. 3 demonstrates that unlike the analogous three dimensional solution for an elliptic lens (Cushman-Roisin, 1987), the pulsation period for an infinite ridge of shallow water does depend on the initial conditions. This is a consequence of the two-dimensional structure of the considered problem, since for any *bounded* shallow water layer the moment of inertia is a finite measure and, according to Ball (1963), follows a harmonic oscillation with the inertial frequency f. For a two-dimensional ridge, the moment of inertia is illdefined and the period of the deformation cycle relates to the three typical evolution patterns discussed in this section.

5. Further remarks

An analytic solution has been derived for the spatio-temporal changes of a two-dimensional shallow water ridge, translating and deforming under the action of gravity, rotation and a uniform external gradient/terrain slope. The solution applies to ridges of parabolic depth profile and linear velocity distribution.

The flow response is a superposition of a solid body translation, induced by the external pressure gradient, and an alternating expansion and contraction between a minimum and a maximum ridge width. Based on the flow fields at one of the extreme expansions, a Rossby number and an inverse rotational Froude number are defined to characterize the deformation component of the response. Unaffected by the uniform external force, the non-harmonic oscillation has a frequency depending on the initial conditions and always larger than the inertial value f. At large inverse Froude numbers (i.e., the gravitational time-scale is much shorter than the inertial period) the fluid ridge initially spreads in the non-rotating limit, and then approaches an asymptotic front velocity.

The detailed features of the flow response certainly must be interpreted in the light of the simplifications concerning the profile and velocity field of the fluid. However the separation property between the translation and deformation components, their relation/independence to uniform pressure gradients and the sensitivity of the pulsation frequency on initial configurations are general results for two-dimensional fluid ridges: Ball (1963) proved the separation for bounded layers of arbitrary depth- and velocity fields, and this theorem can easily be reformulated for two-dimensional layers of any depth/velocity profile. The variation of the pulsation period, depending on the initial configuration, is related to the fact, that for a two-dimensional ridge the moment of inertia is not defined.

The application of analytic solutions to physical phenomena is limited when the solution is unstable to small disturbances. A common method to investigate the stability of solutions is the linear stability analysis. In view of the time-dependent basic state in the present study, such an analysis constitutes a non-trivial mathematical task. Moreover a proper formulation of the stability analysis is difficult, because the linear dynamics is inappropriate in the surrounding of the fronts and an additional boundary condition has to be applied to the disturbances. However two kinds of instabilities are known for a shallow water ridge in geostrophic balance.

The first one, an ageostrophic instability, described by Griffiths et al. (1982), relies upon a coupling between the strong inertial effects at the two front lines. The details of the unstable linear modes depend on the vorticity profiles of the geostrophic basic state. In general e-folding times in the order of one period of the background rotation are achieved and disturbances with a wavelength close to the deformation radius are growing the fastest. The laboratory experiments, reported in the same article, demonstrate that the growing modes consist of a meandering component, longitudinally distorting the ridge into a wavelike form, and a varicose component, alternately thinning and broadening the hump.

A further type of instability is present, when the ridge (in geostrophic basic state) is narrow compared to the deformation radius $L < \sqrt{2gH/f}$, that is, the shear of the flow along the ridge axis is strongly negative and the layer has negative potential vorticity. For such configurations purely two-dimensional disturbances are expected to be unstable due to inertial instability. For the parabolic ridge in consideration an anti-symmetric and a symmetric unstable mode can be distinguished and both of which have a growth rate corresponding to the geometric mean of background- and absolute vorticity: $\sigma = \sqrt{-f(f+V_x)}$.

The flow configuration of the present study is related to various forms of gravity currents commonly observed in geophysical fluids. Examples are density currents, gust fronts, baroclinic fronts and oceanographic lenses. The analytic results can be applied to these phenomena provided non-hydrostatic, frictional and instability effects play a minor role in the flow evolution.

The action of an external pressure gradient for instance is of particular interest in the understanding of orographically trapped density currents. In this context Egger (1989) performed numerical simulations for the motion of a sinusoidal dome in a homogeneous pressure gradient and a non-rotating frame. He reports, that the front velocity relative to the ridge axis was independent of the imposed gradient. This finding is a manifestation of the general splitting property and also holds in a rotating frame.

In the field of thunderstorm research the propagation speed of gust fronts is essential for the understanding of storm maintenance and reformation. Observations (Wakimoto, 1982) and numerical simulations (Thorpe et al., 1980) of gust fronts and also laboratory experiments on density currents (Simpson, 1987) show that the velocity of density fronts often has the form of a gravity current velocity $s\sqrt{gH}$ with a "fudge" factor s between 0.7 and 1. Compared to these findings, the present analytic model with a "fudge" factor of 2 in the asymptotic, non-rotational expansion seems to overestimate the propagation of natural gravity currents. The reason for this discrepancy is unclear, it might be a manifestation of non-hydrostatic and frictional effects present in the head of density fronts in nature.

The temporal evolution of a fluid in a rotating frame, after it is released from an unbalanced flow configuration, is of principal interest in geophysical fluid dynamics and got practical attention in the field of model initialisation. The linear adjustment theory (Gill, 1976) offered the view of gravity waves propagating away and leaving behind a balanced, so called adjusted flow field. Adopting these ideas, numerical weather prediction models are initialized by filtering the divergent flow component from the analysed field. The flow situation in this article now is an example for the *nonlinear* evolution. It demonstrates the principal differences between linear and nonlinear gravity wave propagation that might be important also for model initialisation. In view of the pulsating character of the flow response the name "adjustment" no longer seems appropriate.

Analytic, time-dependent solutions for the nonlinear equations of fluid motion are very rare and only possible for specific flow situations. More complex geophysical fluid dynamics is studies with numerical models, among which the Θ-coordinate formulation became very attractive and physically appealing in the last years. However for this kind of models it is difficult to simulate flow situations where Θ-layers are collapsed or intersect with the ground. In this case "lateral" boundary conditions must be applied in the interior of the model domain and this requires sophisticated numerical algorithms. Since the presented solution analytically predicts the position of a fluid/ground intersection, it constitutes an ideal bench-mark for testing such numerical schemes. The presented solution has recently proven to be very useful in a test of a couple of numerical schemes in a shallow water model (Schär, private communication).

6. Acknowledgement

The author wishes to thank Professor H. C. Davies for initiating this work.

REFERENCES

Ball, F. K. 1963. Some general theorems concerning the finite motion of a shallow rotating liquid lying on a paraboloid. *J. Fluid Mech. 17*, 240–256.

Byrd, P. and Friedman, M. 1954. *Handbook of elliptic integrals for engineers and physicists*. Springer-Verlag, Berlin.

Cushman-Roisin, B. 1987. Exact analytical solutions for elliptical vortices of the shallow-water equations. *Tellus 39A*, 235–244.

Davies, H. C. 1984. On the retardation of a cold front. *Beitr. Phys. Atmosph. 57*, 409–418.

Egger, J. 1989. Föhn and quasi-stationary fronts. *Beitr. Phys. Atmosph. 62*, 20–29.

Gill, A. E. 1976. Adjustment under gravity in a rotating channel. *J. Fluid Mech. 77*, 603–621.

Griffiths, R. W., Killworth, P. D. and Stern, M. E. 1982. Ageostrophic instability of ocean currents. *J. Fluid Mech. 117*, 343–377.

Houghton, D. D. and Kasahara, A. 1968. Nonlinear shallow fluid flow over an isolated ridge. *Comm. Pure Appl. Math. 21*, 1–23.

Laplace, P. S. 1799. 1825. *Méchanique céleste*. Paris.

Orlanski, I. 1968. Instability of frontal waves. *J. Atmos. Sci. 25*, 178–200.

Phillips, N. A. 1954. Energy transformations and meridional circulations associated with simple baroclinic waves in a two-level, quasi-geostrophic model. *Tellus 6*, 273–286.

Simpson, J. E. 1987. *Gravity currents in the environment and the laboratory*. Ellis Horwood series in environmental science, Chichester, England, 244 pp.

Thorpe, A. J., Miller, M. J. and Moncrieff, M. W. 1980. Dynamical models of two-dimensional downdraughts. *Quart. J. R. Met. Soc. 106*, 463–484.

Wakimoto, R. M. 1982. The life cycle of thunderstorm gust fronts as viewed with Doppler radar and rawinsonde data. *Mon. Wea. Rev. 110*, 1060–1082.